The Astrophysical Journal, 809:116 (10pp), 2015 August 20 doi:10.1088/0004-637X/809/2/116

A COMPARATIVE STUDY OF HYPERON EQUATIONS OF STATE IN SUPERNOVA SIMULATIONS

Prasanta Char[1,2], Sarmistha Banik[3], and Debades Bandyopadhyay[1,2]
[1] Astroparticle Physics and Cosmology Division, Saha Institute of Nuclear Physics, 1/AF Bidhannagar, Kolkata-700064, India
[2] Centre for Astroparticle Physics, Saha Institute of Nuclear Physics, 1/AF Bidhannagar, Kolkata-700064, India
[3] BITS Pilani, Hyderabad Campus, Hyderabad-500078, India
Received 2015 April 28; accepted 2015 June 18; published 2015 August 14

ABSTRACT

A comparative study of the Λ hyperon equations of state of Banik, Hempel and Banyopadhyay (BHB), Banik et al., and Shen et al. (denoted as HShen Λ) for core-collapse supernova (CCSN) simulations is carried out in this work. The dynamical evolution of a protoneutron star (PNS) into a black hole is investigated in CCSN simulations in the general relativistic one-dimensional code using the BHB$\Lambda\phi$ and HShen Λ equation of state (EOS) tables and different progenitor models from Woosley & Heger. Radial profiles of the mass fractions of baryons, the density, as well as the temperature in the PNS at different moments in time, are compared for both EOS tables. The behavior of the central density of the PNS with time is demonstrated for these two Λ hyperon EOS tables and compared with their corresponding nuclear EOS tables. It is observed that the black hole formation time is higher in the BHB$\Lambda\phi$ case than in the HShen Λ EOS case for the entire set of progenitor models adopted here, because the repulsive Λ–Λ interaction makes the BHB$\Lambda\phi$ EOS stiffer. Neutrino emission with the Λ hyperon EOS ceases earlier than that of its nuclear counterpart. The long-duration evolution of the shock radius and the gravitational mass of the PNS after a successful supernova explosion with enhanced neutrino heating are studied with the BHB$\Lambda\phi$ EOS and *s*20WH07 progenitor model. The PNS is found to remain stable for 4 s and might evolve into a cold neutron star.

Key words: equation of state – stars: black holes – stars: neutron – supernovae: general

1. INTRODUCTION

The recent discovery of a 2 $M_\odot$ neutron star puts stringent conditions on the composition and equation of state (EOS) for dense matter in neutron star interiors (Antoniadis et al. 2013). It has been observed that the presence of strange degrees of freedom such as hyperons makes the EOS softer, which is incompatible with the massive neutron star in most cases. This is known as the hyperon puzzle (Buballa et al. 2014; Lonardoni et al. 2015). Describing hyperon matter in neutron stars is a challenge for many-body theories. It has been argued that the hyperon–hyperon repulsive interaction due to the exchange of a strange vector meson makes the EOS stiffer and might overcome the puzzle.

The β-equilibrated equations of state that include hyperons were constructed after the discovery of the massive neutron star by several groups. Those hyperon equations of state are found to result in 2 $M_\odot$ or heavier neutron stars (Lastowiecki et al. 2012; Weissenborn et al. 2012a, 2012b; Colucci & Sedrakian 2013; Lopes & Menezes 2013; Char & Banik 2014; Gusakov et al. 2014; van Dalen et al. 2014). Besides hyperons, the antikaon condensate was also included in some calculations, which led to massive neutron stars (Char & Banik 2014). In all of these calculations, the repulsive hyperon–hyperon interaction that is mediated by ϕ mesons was considered.

Many EOS tables involving hyperons were developed for supernova simulations. The first hyperon EOS table was prepared by Ishizuka et al. (2008). In this case, the full baryon octet was added to the Shen nucleon EOS table (Shen et al. 1998; Ishizuka et al. 2008). The Shen nucleon EOS table was based on a relativistic mean field (RMF) model that had the Thomas–Fermi approximation for the description of inhomogeneous matter below the saturation density (Shen et al. 1998). Later, the Shen nucleon EOS was extended to include only Λ hyperons in the HShen Λ EOS table (Shen et al. 2011). Another extensively used supernova EOS is the Lattimer and Swesty (LS) nucleon EOS table, which based on the non-relativistic Skyrme interaction (Lattimer & Swesty 1991). Recently, Λ hyperons were included in the LS nucleon EOS (Oertel et al. 2012). All of these hyperon EOS tables were used in core-collapse supernova (CCSN) simulations by several authors (Ishizuka et al. 2008; Nakazato et al. 2008, 2012; Sumiyoshi et al. 2009; Banik 2013, 2014). However, none of these hyperon EOS tables were consistent with the 2 $M_\odot$ neutron star constraint.

Recently, we computed EOS tables that included Λ hyperons within the framework of the density dependent relativistic hadron (DDRH) field theory (Banik et al. 2014). In those EOS tables, light and heavy nuclei, as well as interacting nucleons, are described in the nuclear statistical equilibrium (NSE) model, which takes into account the excluded volume effects (Hempel & Schaffner-Bielich 2010; Banik et al. 2014). Two variants of the hyperon EOS tables were generated—in one case (Banik, Hempel and Banyopadhyay; BHB$\Lambda\phi$) the repulsive Λ hyperon–Λ hyperon interaction mediated by ϕ mesons was considered, and in the other case (BHBΛ) this interaction was neglected. It should be noted that the DDRH model with the DD2 parameter set for nucleons is in very good agreement with the symmetry energy properties at the saturation density (Typel et al. 2010, 2013; Lattimer & Lim 2013). We imposed the charge neutrality and β-equilibrium conditions on the BHB hyperon EOS tables and calculated the mass–radius relationship of the neutron star sequence. It was observed that the maximum mass corresponding to the BHB$\Lambda\phi$ EOS was 2.1 $M_\odot$, which is well above the recently observed massive neutron star (Banik et al. 2014). Other hyperon EOSs for β-equilibrated neutron star matter gave rise to the maximum-mass neutron stars of 1.75 $M_\odot$ for the HShen Λ EOS (Shen et al. 2011), 1.6 $M_\odot$ for Ishizuka EOS (Ishizuka

et al. 2008), and 1.91 $M_{\odot}$ for the LS+Λ EOS (Oertel et al. 2012).

In this paper, for the first time, we perform supernova simulations with the BHBΛφ EOS table, which is compatible with a 2 $M_{\odot}$ neutron star, in the general relativistic one-dimensional (GR1D; O'Connor & Ott 2010) hydrodynamics code. Our main goal is to investigate the appearance of Λ hyperons in the postbounce phase and the role of Λ hyperons in CCSNs. Furthermore, we compare our simulation results with those of previous calculations with other hyperon EOS tables, particularly the HShen Λ EOS table (Banik 2013). We are looking for important effects of hyperons in CCSN with the BHBΛφ EOS compared with those of other hyperon EOS.

The paper is organized as follows. In Section 2, the DDRH model for the BHBΛφ EOS table and the RMF model for the HShen Λ EOS table are described. We also briefly discuss the GR1D model for CCSN simulations. The results of our calculation are discussed and compared with those of the HShen Λ EOS in Section 3. Section 4 contains the summary and conclusions.

2. METHODOLOGY

First we shall discuss the salient feature of the BHBΛφ and HShen Λ EOS tables for CCSN simulations (Shen et al. 2011; Banik et al. 2014). The EOS tables are functions of three parameters, i.e., baryon number density, temperature, and proton fraction. In both cases, the compositions of matter that vary from one region to the other depending on those parameters are nuclei, (anti)neutrons, (anti)protons, (anti)Λ hyperons, photons, and electrons and positrons that form a uniform background. The contribution of (anti)neutrinos is not added to the EOS tables and is dealt with separately. We describe the baryonic contribution below.

2.1. BHBΛφ and HShen Λ EOS tables

In the BHBΛφ EOS table, the nuclear statistical equilibrium (NSE) model of Hempel & Schaffner-Bielich (2010) is applied for the description of the matter made of light and heavy nuclei, and unbound nucleons at low temperatures and below the saturation density, whereas the high-density matter is described within the framework of the DDRH model adopting the RMF approximation (Banik & Bandyopadhyay 2002; Typel et al. 2010; Banik et al. 2014). The repulsive interaction between Λ hyperons mediated by φ mesons is included in the RMF model. Nucleon–meson couplings in the DDRH model are density dependent. The DD2 parameter set of nucleon–meson couplings is used to describe the nuclear matter properties (Typel & Wolter 1999; Typel et al. 2010, 2013; Fischer et al. 2014). It should be noted that the nuclear EOS in the DDRH model using DD2 parameter set is known as HS(DD2) (Fischer et al. 2014).

On the other hand, the uniform matter at high density and temperature in the HShen Λ EOS table was described within the framework of the RMF model including nonlinear terms in σ and ω mesons (Shen et al. 2011); non-uniform matter at low temperatures and below the saturation density was considered as a mixture of alpha particles, heavy nuclei, and unbound nucleons. Heavy nuclei were calculated using the Thomas–Fermi approach. The Shen EOS exploited the single nucleus approximation for heavy nuclei (Shen et al. 1998, 2011). The interaction among Λ hyperons due to φ mesons was neglected in this case. Furthermore, in this case baryon–meson couplings of the RMF model are density-independent. We denote the EOSs with and without Λ hyperons as HShen Λ and HShen, respectively. The parameter set from Sugahara & Toki (1994) that is known as the TM1 set was adopted for the nucleon–meson coupling constants of the RMF model.

Table 1
The Saturation Properties of Nuclear Matter such as Saturation Density (n_0), Binding Energy (BE), Incompressibility (K), Symmetry Energy (S), and Slope Coefficient of Symmetry Energy (L) Are Obtained Using the DD2 and TM1 Parameter Sets

Parameter Set	n_0 (fm^{-3})	BE (MeV)	K (MeV)	S (MeV)	L (MeV)	$M_{\rm max}$ ($M_{\odot}$)
DD2	0.1491	16.02	243	31.67	55.04	2.42
TM1	0.1455	16.31	281	36.95	110.99	2.18

Note. Maximum masses of cold neutron stars without Λ hyperons corresponding to HS(DD2) and HShen EOS are also mentioned here.

The nuclear matter saturation properties of the two RMF models discussed above are recorded in Table 1. It should be noted that though the incompressibility of nuclear matter, symmetry energy, and its slope coefficient of the DD2 set at the saturation density are in very good agreement with experimental values (Lattimer & Lim 2013; Fischer et al. 2014), the corresponding quantities of the TM1 set are not. This would have serious bearing on the description of high-density matter in the RMF model of HShen (Shen et al. 2011). For both EOS tables, Λ hyperon–vector meson couplings are estimated from the SU(6) symmetry relations (Dover & Gal 1985; Schaffner & Mishustin 1996) and Λ hyperon–scalar meson coupling is obtained from the hypernuclei data. The Λ hyperon potential depth is −30 MeV in normal nuclear matter (Millener et al. 1988; Schaffner et al. 1992; Mares et al. 1995).

The EOSs of β-equilibrated and charge-neutral cold neutron star matter with and without Λ hyperons are calculated from the supernova EOS tables. The maximum masses of cold neutron stars without Λ hyperons for the HS(DD2) and HShen EOS are given by Table 1. Furthermore, the maximum masses of cold neutron stars corresponding to BHBΛφ and HShen Λ are 2.1 $M_{\odot}$ and 1.75 $M_{\odot}$ (Shen et al. 2011; Banik et al. 2014), respectively.

For CCSN simulations, we make use of the HS(DD2), BHBΛφ, HShen, and HShen Λ EOS tables, which are available from the stellarcollapse.org website.[4]

2.2. General Relativistic Model for Supernova Simulations

We perform the CCSN simulations using the spherically symmetric general relativistic hydrodynamics code GR1D, which was developed by O'Connor & Ott (2010). Microphysical EOSs for supernova matter and an approximate treatment of neutrinos in the pre- and postbounce phases are implemented in the GR1D code. We use the BHBΛφ and HShen Λ EOS tables in CCSN simulations with the GR1D code. Three neutrino species, denoted by "ν_e," $\bar{\nu}_e$ $\nu_x (=\nu_\mu, \bar{\nu}_\mu, \nu_\tau, \bar{\nu}_\tau)$, are considered in this model (O'Connor & Ott 2011). Key aspects of neutrino heating and cooling are incorporated into the model. The leakage scheme (Ruffert et al. 1996; Rosswog & Liebendörfer 2003) exploited in the GR1D code gives approximate number and energy emission

[4] See http://stellarcollapse.org/equationofstate

Table 2
Black Hole Formation Time and Baryonic and Gravitational Masses of PNSs for CCSN Simulations with the Progenitor Models of Woosley & Heger (2007) and the BHB$\Lambda\phi$ and HShen Λ EOS Tables

Model	BHB$\Lambda\phi$			HShen Λ		
	$t_{\rm BH}$ (s)	$M_{b,\rm max}$ ($M_\odot$)	$M_{g,\rm max}$ ($M_\odot$)	$t_{\rm BH}$ (s)	$M_{b,\rm max}$ ($M_\odot$)	$M_{g,\rm max}$ ($M_\odot$)
s20WH07	1.938	2.251	2.138	1.652	1.999	1.964
s23WH07	0.879	2.276	2.203	0.847	2.095	2.073
s25WH07	1.548	2.234	2.141	1.376	2.035	2.001
s30WH07	2.942	2.243	2.113	2.258	1.967	1.929
s35WH07	1.175	2.243	2.161	1.084	2.071	2.041
s40WH07	0.555	2.250	2.210	0.565	2.129	2.118

Note. For all cases considered here, $f_{\rm heat} = 1$.

rates. The neutrino heating rate considered here involves the scale factor $f_{\rm heat}$, which could be enhanced beyond the normal value of 1 to achieve additional neutrino heating for "successful" CCSN explosions (Janka 2001; O'Connor & Ott 2011). We take $f_{\rm heat} = 1$ in CCSN simulations, if not stated otherwise.

In principle an accurate and expensive neutrino treatment should be based on the Boltzmann neutrino transport. However, computationally efficient schemes for neutrinos are employed in the GR1D code for faster CCSN simulations. Moreover, it has been noted that the results obtained in CCSN simulations using the simplified treatment of neutrino leakage and heating in the GR1D were quantitatively similar to the results obtained from one-dimensional (1D) simulations with the Boltzmann neutrino transport by other groups (Fischer et al. 2009; Sumiyoshi et al. 2009). It was argued that progenitor structures played more important roles in the collapse of a protoneutron star (PNS) to a black hole than the details of neutrino treatment (O'Connor & Ott 2011).

3. RESULTS AND DISCUSSION

Now we report our investigations of CCSNs within the GR1D code using the HShen Λ hyperon and BHB$\Lambda\phi$ EOS tables. In these studies, nonrotating progenitors of Woosley & Heger (2007; WH07) are used. In their stellar evolution studies Woosley & Heger (2007) evolved zero-age main-sequence (ZAMS) stars, with solar metallicity denoted by the prefix s before presupernova models, followed by ZAMS mass. Significant mass loss was reported in sWH07 presupernova models (O'Connor & Ott 2011).

We perform the CCSN simulations with presupernova models as recorded in Table 2. In all numerical calculations, we fix the neutrino heating factor $f_{\rm heat} = 1$. In the next paragraphs, we discuss the results of simulations starting from the gravitational collapse of the iron core followed by the core bounce to the postbounce evolution of the PNS for s40WH07 and s23WH07 models with the HShen Λ and BHB$\Lambda\phi$ EOS tables in details. In all of these simulations, a shock wave is launched at the core bounce, stalls after traversing a few 100 km, then recedes and becomes an accretion shock. Because neutrinos in the 1D CCSN model could not revive the shock, the PNS shrinks due to mass accretion and its density and temperature increase during the postbounce evolution. This leads to the appearance of Λ hyperons in the PNS.

For s40WH07, the core bounce occurs at 0.273 and 0.321 s, corresponding to the HShen Λ hyperon and the BHB$\Lambda\phi$ EOS, respectively. Similarly, in *the* s23WH07 model the core bounce times for the HShen Λ and the BHB$\Lambda\phi$ EOS are 0.266 and 0.315 s, respectively. The appearance of strangeness or Λ hyperons in the postbounce phase and its role in the evolution of the PNS are the main focuses of this investigation. For s40WH07 and s23WH07 models and both hyperon EOS tables, Λ hyperons do not populate the PNS at the core bounce. In simulations with both presupernova models, strangeness in the form of Λ hyperons sets in a few hundred milliseconds (ms) after the core bounce and increases with time thereafter.

Figure 1 depicts the PNS compositions as a function of radius at two different postbounce times for s40WH07 with the HShen Λ (left panel) and BHB$\Lambda\phi$ (right panel) EOS tables. For postbounce time ($t_{\rm pb}$) 0.31 s, the central value of Λ fraction is higher for the BHB$\Lambda\phi$ EOS than that of the HShen Λ hyperon EOS. The profile of Λ hyperons is wider in the latter case. We find similar trends for Λ hyperons at a later time $t_{\rm pb} = 0.51$ s. For both EOS tables, the population of Λs increases with time. It is to be noted that the central value of the Λ fraction is a high-density effect, whereas the off-center Λs are populated thermally. We study the density and temperature profiles to understand this behavior.

The density profiles as a function of radius are plotted for s40HW07 at the bounce as well as for $t_{\rm pb} = 0.31$ and 0.51 s in Figure 2. The left panel of the figure corresponds to the HShen Λ EOS and the right panel implies the results of the BHB$\Lambda\phi$ EOS. At the bounce, the central density ($\rho_{\rm c}$) of the PNS in both cases is just above the normal nuclear matter density, as evidenced by the figure. Though the density profiles for both EOS tables are quantitatively the same at $t_{\rm pb} = 0$, they differ at later times. The central density at $t_{\rm pb} = 0.51$ in the right panel is higher than that of the left panel. In both cases, the central density exceeds two times the normal nuclear matter density. This high central density facilitates a significant population of Λs in the core of the PNS, as seen in Figure 1. However, the density falls well below normal nuclear matter density at the tail of the profile. The off-center Λs in Figure 1 could not be attributed to the density effect.

The temperature profiles as a function of radius are shown for s40WH07, with the HShen Λ hyperon (left panel) and the BHB$\Lambda\phi$ (right panel) EOS tables in Figure 3. Just as in Figure 2, the temperatures profiles are plotted at the core bounce and $t_{\rm pb} = 0.31$ and 0.51 s in both panels of Figure 3. The peaks of the temperature profiles located away from the center of the PNS for both EOSs after the core bounce later shift toward the center with time in both panels. It is to be noted that the central temperature at the bounce is higher for the BHB$\Lambda\phi$ EOS compared with the corresponding temperature for the HShen Λ EOS. Furthermore, the peak temperature around 8 km at 0.51 s after core bounce in the case of the BHB$\Lambda\phi$ EOS is much higher than the corresponding scenario for the HShen Λ EOS. This high temperature results in thermally produced Λ hyperons away from the center of the PNS as shown in Figure 1. We find from Figure 1 that thermal Λs are more abundant around 8 km at later times for the BHB$\Lambda\phi$ EOS due to a higher peak temperature.

We also study profiles of particle fraction, density, and temperature for s23WH07 using both hyperon EOS tables as shown in Figures 4–6. We obtain qualitatively similar results for s23WH07, as we have already discussed for s40WH07.

Now we focus on the postbounce evolution of the PNS for different presupernova models with nuclear and Λ hyperon

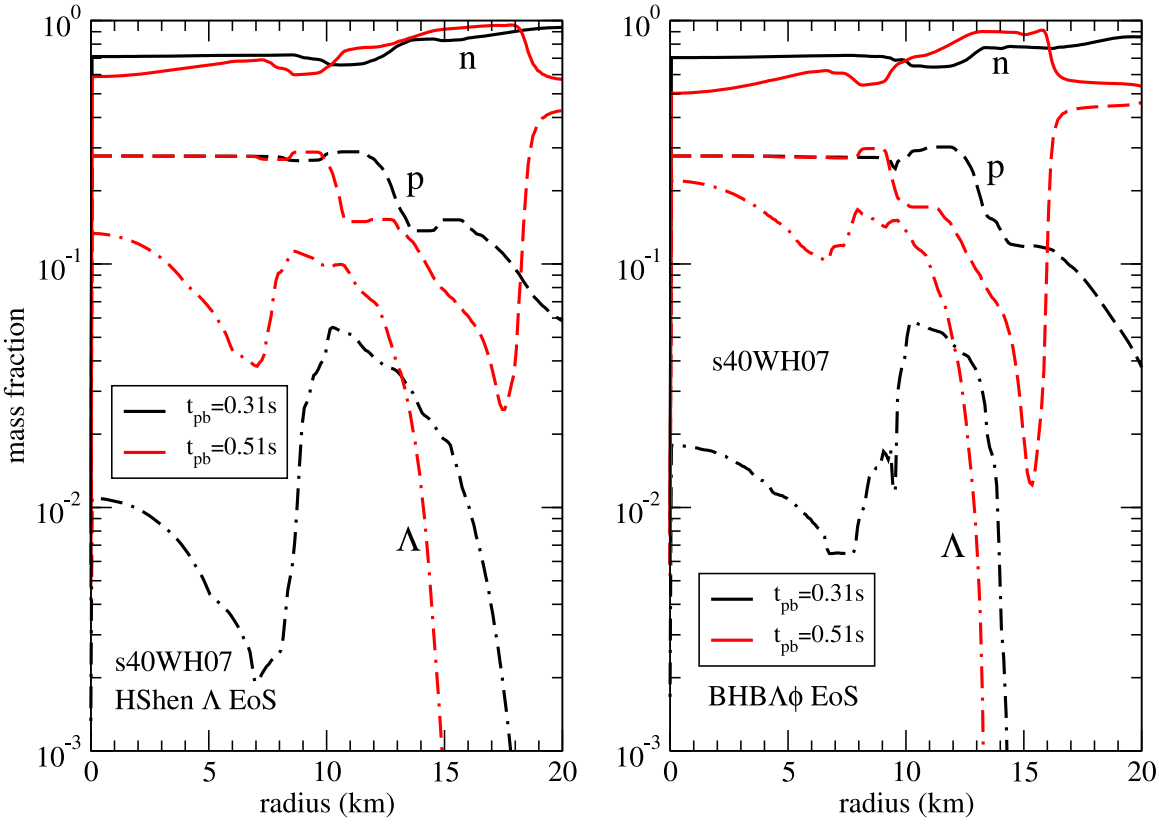

Figure 1. Mass fractions of different species in the PNS are shown as a function of radius for the HShen Λ EOS (left panel) and the BHBΛϕ EOS (right panel) at t_{pb} = 0.31 and 0.51 s (online-version: red). The results in both panels correspond to the *s*40WH07 model.

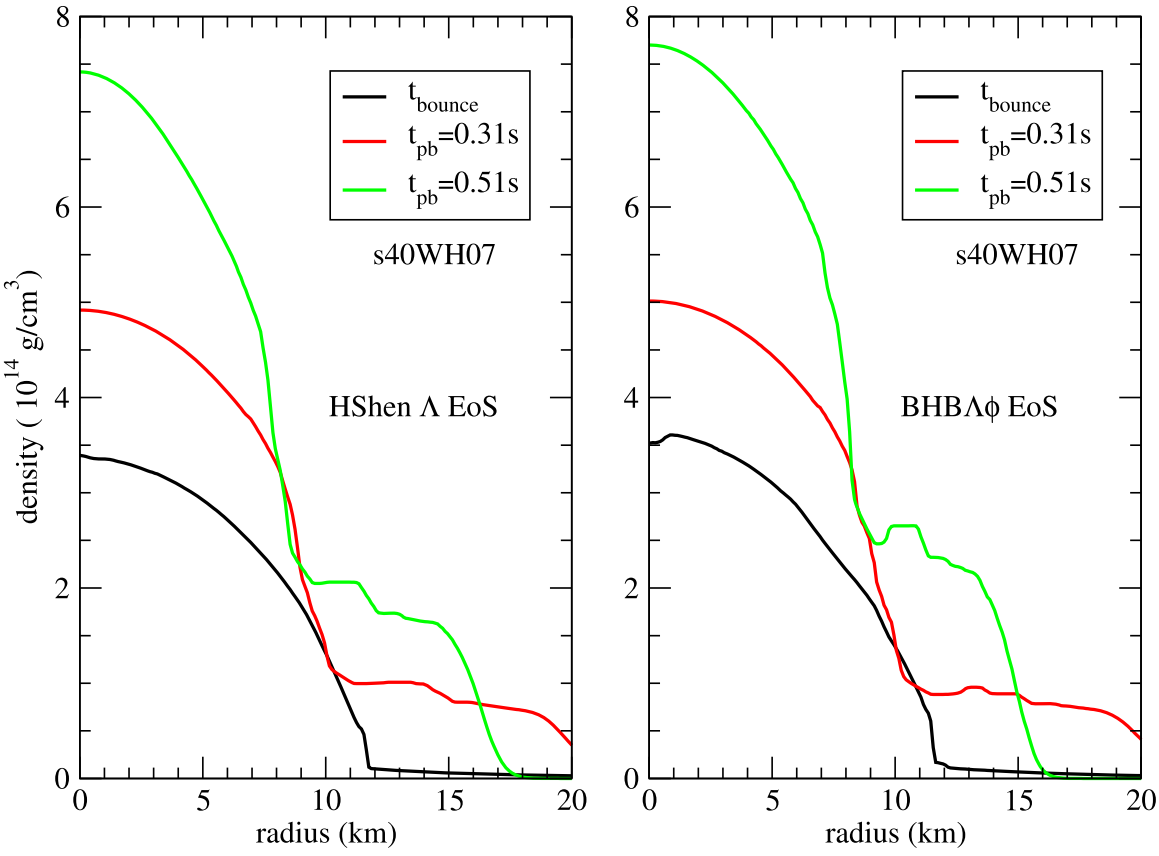

Figure 2. Density profiles of the PNS are shown as a function of radius for the HShen Λ EOS (left panel) and the BHBΛϕ EOS (right panel) at the core bounce and t_{pb} = 0.31 (online-version: red) and 0.51 s (online-version: green). The results in both panels correspond to the *s*40WH07 model.

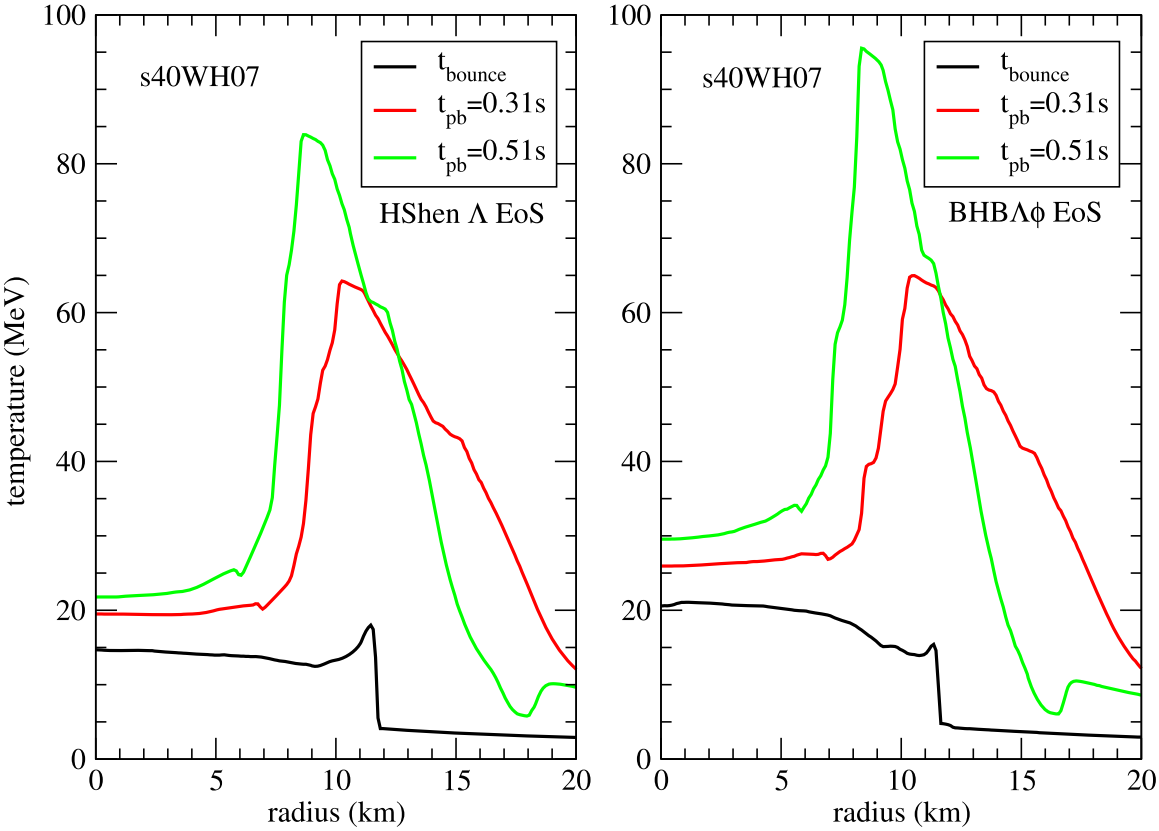

Figure 3. Temperature profiles of the PNS are shown as a function of radius for the HShen Λ EOS (left panel) and the BHBΛϕ EOS (right panel) at the core bounce and $t_{pb} = 0.31$ (online-version: red) and 0.51 s (online-version: green). The results in both panels correspond to the *s*40WH07 model.

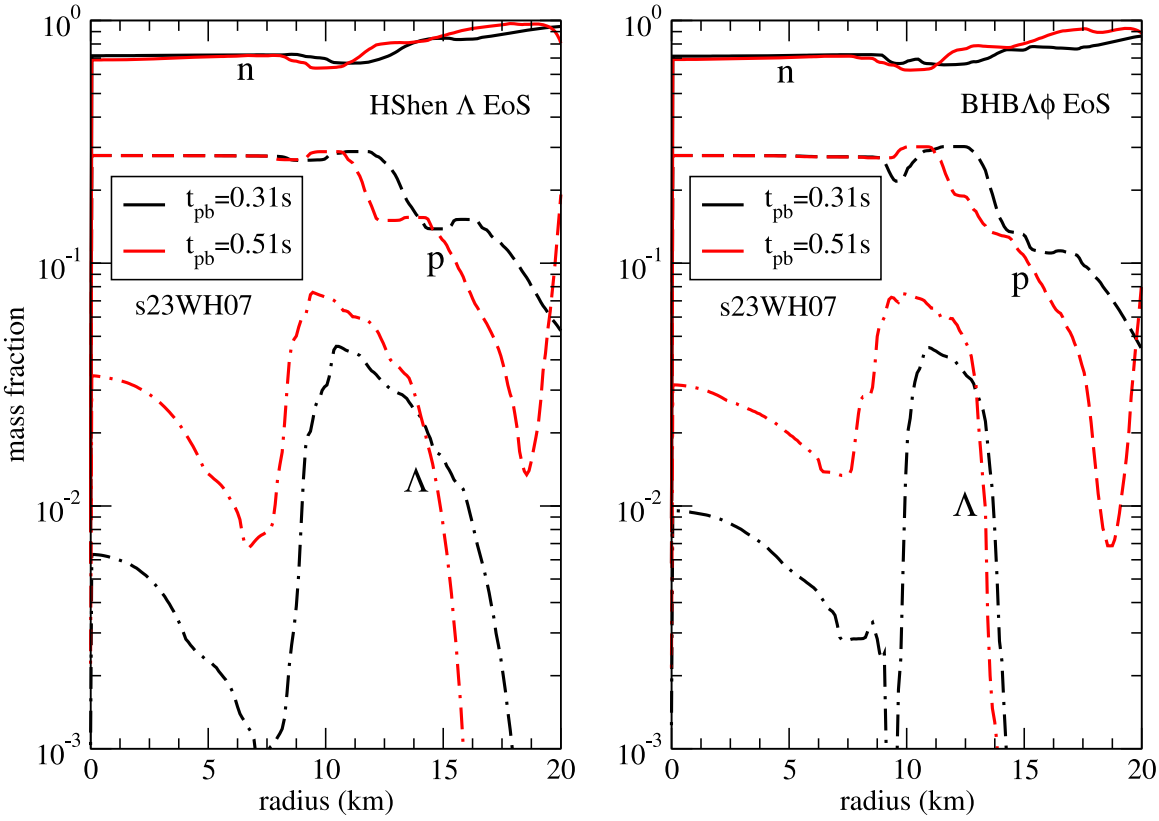

Figure 4. Same as Figure 1 but for the *s*23WH07 model. The results correspond to the HShen Λ EOS (left panel) and the BHBΛϕ EOS (right panel) at $t_{pb} = 0.31$ and 0.51 s (online-version: red).

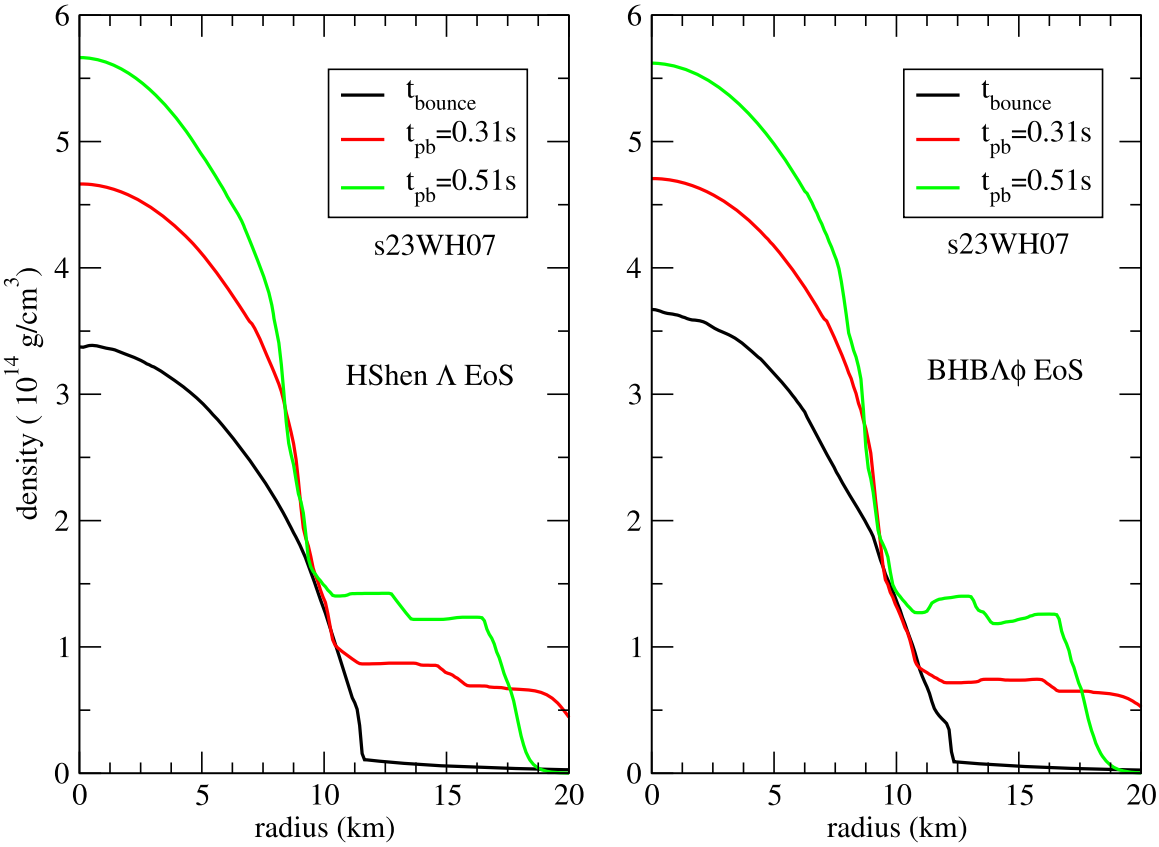

Figure 5. Same as Figure 2 but for the *s*23WH07 model. The results correspond to the HShen Λ EOS (left panel) and the BHBΛϕ EOS (right panel) at the core bounce and $t_{pb} = 0.31$ (online-version: red) and 0.51 s (online-version: green).

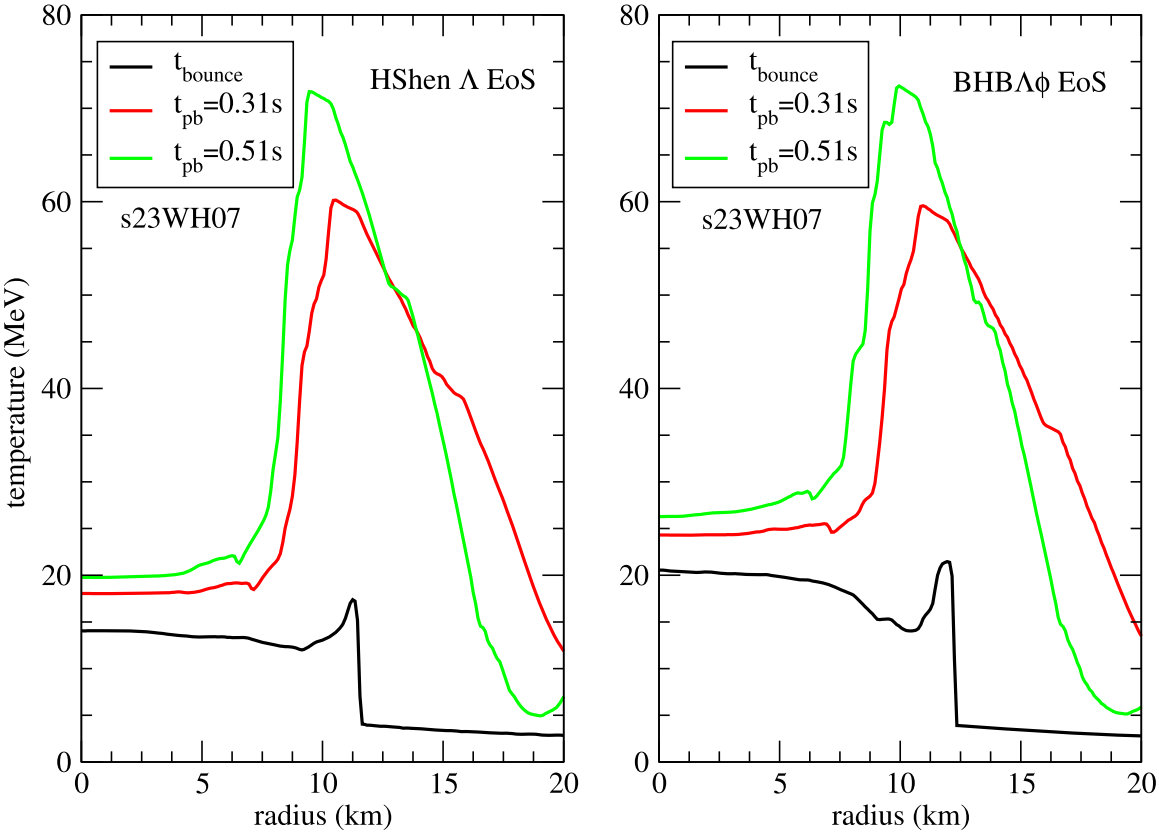

Figure 6. Same as Figure 3 but for the *s*23WH07 model. The results correspond to the HShen Λ EOS (left panel) and the BHBΛϕ EOS (right panel) at the core bounce and $t_{pb} = 0.31$ (online-version: red) and 0.51 s (online-version: green).

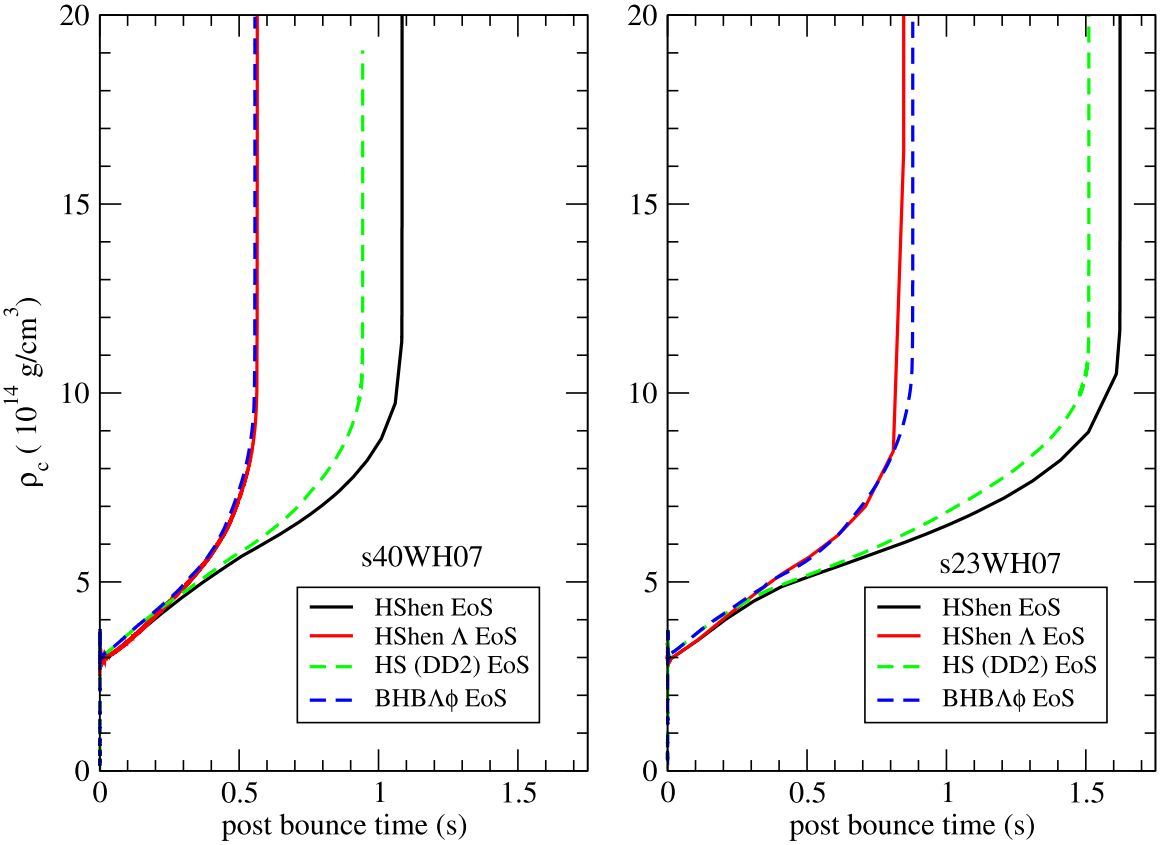

Figure 7. Central baryon density is plotted with postbounce time for the HShen nuclear EOS, the HShen Λ EOS (online-version: red), the HS(DD2) (online-version: green) and the BHBΛϕ EOS (online-version: blue). The results in the left and right panels correspond to the *s*40WH07 and *s*23WH07 models.

EOS tables corresponding to the HShen and BHB models. Figure 7 exhibits the evolution of the central density of the PNS with the postbounce times for *s*40WH07 (left panel) and *s*23WH07 (right panel). Results are shown in both panels for the HShen nuclear EOS, the HShen Λ EOS, the HS(DD2) nuclear EOS, and the BHBΛϕ EOS. It should be noted that the core bounce time for the hyperon EOS is the same as that of the corresponding nuclear EOS. In all cases, in both panels of Figure 7 we find that the central density increases gradually to several times the normal nuclear matter density. Finally, there is a steep rise in the central density when the PNS dynamically collapses into a black hole in milliseconds. It should be noted that the black hole formation time is different for different EOS models. It is evident from the CCSN simulation of *s*23WH07 that the black holes are formed at 1.511 and 1.623 s after the core bounce for the HS(DD2) and the HShen EOS, respectively. For *s*40WH07 the black hole formation time is 0.942 s in the case of the HS(DD2) EOS, whereas it is 1.084 s for the HShen EOS. For both supernova models and nuclear EOS tables, the black hole is formed earlier in the case of the HS(DD2) than the situation with the HShen EOS. The maximum gravitational (baryonic) PNS masses are 2.464 (2.616) $M_\odot$ and 2.459 (2.587) $M_\odot$ for *s*40SW07 with the HS (DD2) and the HShen EOS, respectively. Similarly, for *s*23WH07, those are 2.428 (2.605) $M_\odot$ and 2.383 (2.512) $M_\odot$ corresponding to the HS(DD2) and the HShen EOS. On the other hand, the dynamical collapse to a black hole is accelerated for the HShen Λ and the BHBΛϕ EOS tables because hyperons make the EOS softer. It is evident from Figure 7 that the black hole formation time is shorter for hyperon EOS than for the corresponding nuclear EOS. However, there is little difference between the black hole formation times corresponding to the HShen Λ and BHBΛϕ EOSs.

The results of CCSN simulations with other presupernova models are recorded in Table 2. The first column of the table lists the presupernova models of Woosley & Heger (2007), starting from *s*20WH07 to *s*40WH07. Two EOS tables, such as the HShen Λ and the BHBΛϕ, are adopted in these calculations. Under each EOS, the first column represents the black hole formation time ($t_{\rm BH}$) estimated from the core bounce and the next column gives the maximum baryon mass ($M_{b,\rm max}$), followed by the maximum gravitational mass ($M_{g,\rm max}$) of the PNS at the point of instability corresponding to the central value of the lapse function 0.3. Further investigations with the two Λ hyperon EOSs reveal an opposite behavior of $t_{\rm BH}$ than what has been observed for nuclear EOSs. For Λ hyperon EOS, $t_{\rm BH}$ for the BHBΛϕ is always greater than that of the HShen Λ for all presupernova models except *s*40WH07. The comparison of two hyperon EOSs shows that the BHBΛϕ is a stiffer EOS than the HShen Λ. The explanation of this behavior may be traced back to the inclusion of repulsive Λ–Λ interaction in the BHBΛϕ EOS. For all presupernova models and EOSs adopted in simulations, it is evident from the table that the maximum gravitational mass of the PNSs in each case is higher than their corresponding maximum cold neutron star masses. However, in some cases the maximum gravitational mass of the PNS collapsing into a black hole with the HShen Λ EOS is less than the two solar mass limit because the HShen Λ EOS does not result in a 2 $M_\odot$ cold neutron star. It is interesting to note that in

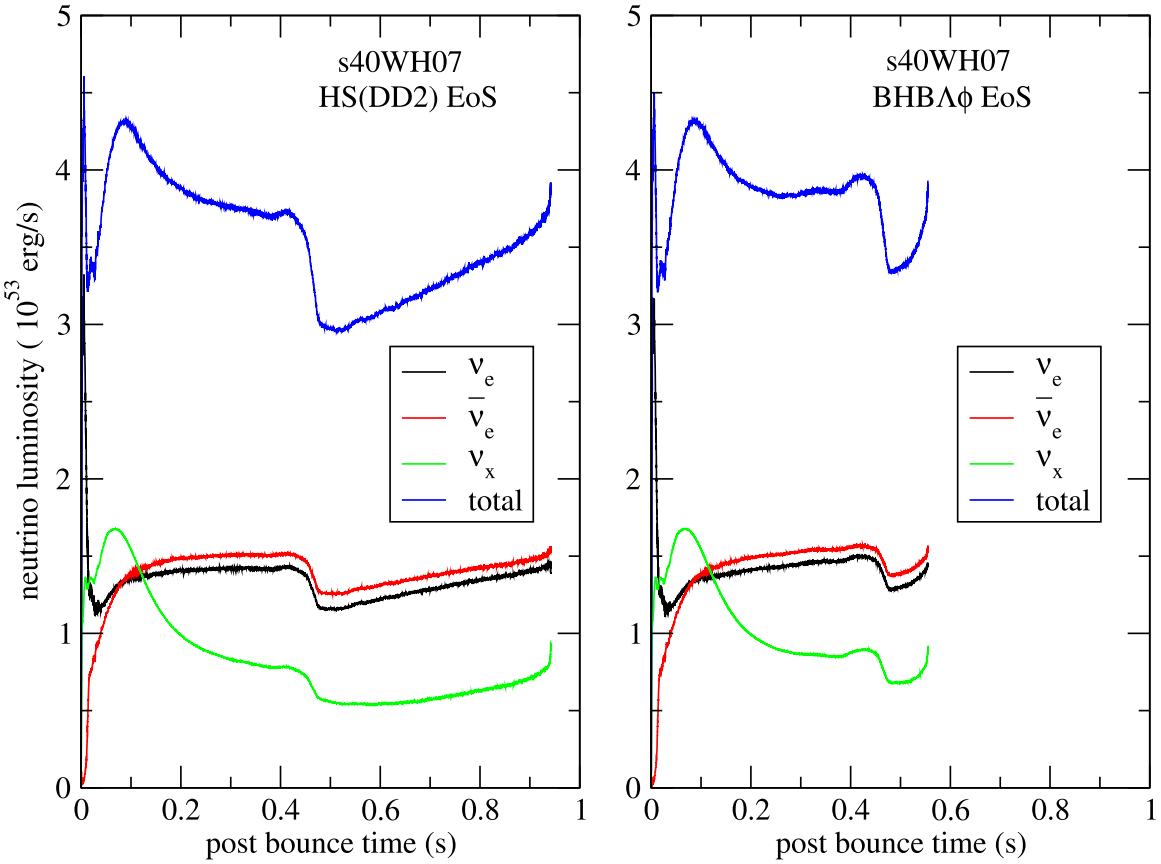

Figure 8. Total neutrino luminosity (online-version: blue) as well as ν_e, $\bar{\nu}_e$ (online-version: red), and ν_x (online-version: green) luminosities are plotted with the postbounce time for the HS(DD2) (left panel) and the BHB$\Lambda\phi$ (right panel) EOS. The results correspond to the s40WH07 model.

the case of the HShen Λ EOS, the difference between $M_{g,\max}$ of the PNS and the maximum mass of the cold neutron star that includes Λ hyperons (1.75 $M_\odot$) is appreciable, whereas the maximum gravitational mass of the PNS for the BHB$\Lambda\phi$ EOS is very similar to the value of the corresponding maximum mass of the cold neutron star with Λs (2.1 $M_\odot$) for the entire set of progenitor models. This shows that the thermal effects in the PNS for the BHBH$\Lambda\phi$ might not be as strong as in the PNS with the HShenΛ because the EOS is stiffer in the former case. The role of decreasing thermal pressure with increasing stiffness of the EOS was already noted by O'Connor & Ott (2011). This should have interesting implications for the study of the metastability of the PNS with the BHB$\Lambda\phi$ EOS.

We compare our findings with other CCSN simulations with hyperon EOS. The Ishizuka hyperon EOS includes Λ, Σ, and Ξ hyperons and is an extension of the HShen nuclear EOS (Ishizuka et al. 2008). The CCSN simulations were performed in a spherically symmetric general relativistic neutrino radiation hydrodynamics model using a 40 $M_\odot$ progenitor of Woosley & Weaver (1995) and the Ishizuka hyperon EOS (Sumiyoshi et al. 2009; Nakazato et al. 2012). With the LS+Λ EOS, (Oertel et al. 2012) Peres et al. (2013) carried out a similar investigation using an s40WW progenitor and a low-metallicity 40 $M_\odot$ progenitor of Woosley et al. (2002) called u40. Banik (2013) also studied CCSN simulations using the HShen Λ EOS and progenitor models of Woosley & Heger (2007), particularly studying the long-duration evolution of the PNS in the context of understanding the fate of the compact object in SN1987A. It should be noted that though our results with the BHB$\Lambda\phi$ EOS are qualitatively similar to those of earlier calculations, they are quantitatively different because only our Λ hyperon EOS is compatible with the 2 $M_\odot$ limit of cold neutron stars. The early black hole formation due to softening in the Λ hyperon EOS compared with the nuclear EOS is a robust conclusion in all of these calculations. Total neutrino luminosity as well as ν_e, $\bar{\nu}_e$, and ν_x luminosities as a function of postbounce time are plotted in Figure 8 for the HS(DD2) (left panel) and the BHB$\Lambda\phi$ (right panel) EOS. The results are shown here for the s40WH07 model. It should be noted that the neutrino emission ceases earlier for the BHB$\Lambda\phi$ case than for the scenario with the HS(DD2) nuclear EOS. A similar conclusion was arrived at in the simulation with other hyperon EOSs (Sumiyoshi et al. 2009; Banik 2013). The shorter neutrino burst corresponding to the Λ hyperon EOS before the collapse of the PNS into the black hole could be an important probe for the appearance of Λ hyperons in the PNS. This demands a more accurate treatment of neutrinos in the GR1D code. Figure 9 exhibits the neutrino luminosities for both the Λ hyperon EOS and the s40WH07 model. We find similar features for neutrino luminosities for both cases. Though we are considering a phase transition from nuclear to Λ hyperon matter, we do not find any evidence for a second neutrino burst, which was observed in a first-order quark-hadron phase and was responsible for a successful supernova explosion (Sagert et al. 2009).

So far we have seen that simulations in the 1D CCSN model might lead to accretion-driven black holes in failed supernovae. If a successful supernova occurs, can exotic matter such as

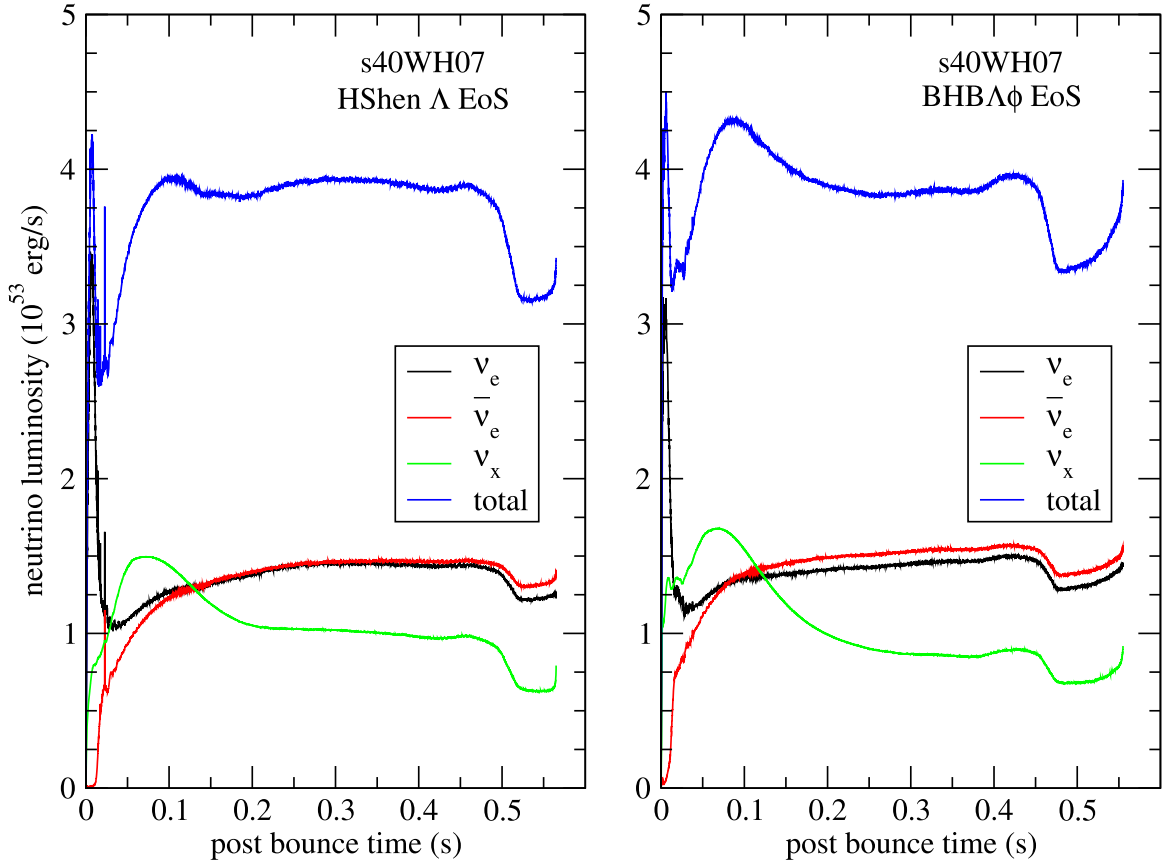

Figure 9. Total neutrino luminosity (online-version: blue) as well as ν_e, $\bar{\nu}_e$ (online-version: red), and ν_x (online-version: green) luminosities are plotted with the postbounce time for the HShen Λ (left panel) and the BHBΛϕ (right panel) EOS. The results correspond to the *s*40WH07 model.

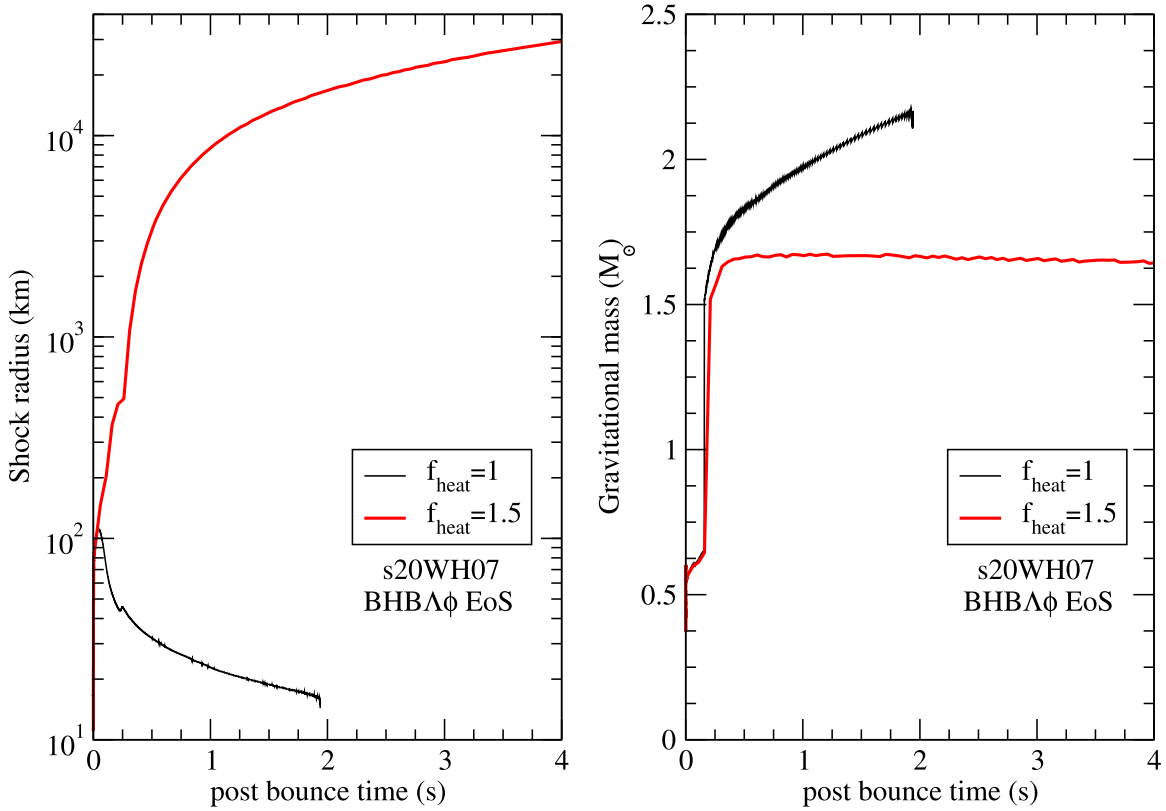

Figure 10. Shock radius (left panel) and gravitational mass of the PNS (right panel) are plotted with postbounce time using the neutrino heating factor $f_{heat} = 1$ and 1.5 (online-version: red) for the *s*20WH07 model and the BHBΛϕ EOS.

hyperons make the PNS metastable and drive it to become a low-mass black hole during the long-duration evolution when thermal support decreases and deleptonization takes place in the PNS? Such a scenario was envisaged for the non-observation of a compact object in SN1987A (Brown & Bethe 1994; Prakash et al. 1995; Banik & Bandyopadhyay 2001). This problem was also studied in CCSN simulations (Keil & Janka 1995; Baumgarte et al. 1996; Banik 2013). We continue our study by increasing the neutrino heating scale factor to $f_{\rm heat} = 1.5$ for s20WH07 with the BHB$\Lambda\phi$ EOS. The left panel of Figure 10 exhibits the shock radius as a function of postbounce time. For the neutrino scale factor $f_{\rm heat} = 1$, it fails to launch a successful supernova explosion and the shock radius recedes. Finally, the PNS collapses into a black hole. For $f_{\rm heat} = 1.5$ it is observed that the shock radius increases with time after a successful supernova explosion. The PNS remains stable until 4 s. We do not find any onset of the metastability in the PNS due to the loss of thermal support and neutrino pressure during the cooling phase over a few seconds. The window for the metastability is very narrow because the maximum PNS mass in this case is 2.138 $M_\odot$, whereas the maximum cold neutron star mass corresponding to the BHB$\Lambda\phi$ EOS is 2.1 $M_\odot$. The PNS might evolve into a cold neutron star. Gravitational masses of the PNS for $f_{\rm heat} = 1$ and 1.5 are shown as a function of postbounce time in the right panel of Figure 10. The PNS cools down to a neutron star with a mass $\sim$1.64 $M_\odot$ at the end of 4 s.

4. SUMMARY AND CONCLUSIONS

We have performed CCSN simulations using the BHB$\Lambda\phi$ EOS, which is compatible with a 2 $M_\odot$ neutron star, and several progenitor models from the stellar studies of Woosley & Heger (2007). It is observed that Λs are produced a few hundred milliseconds after the core bounce. The appearance of Λ hyperons is studied in great detail. It is evident from the density and temperature profiles as a function of radius that Λs are produced in the core of the PNS when the central density exceeds two times the normal nuclear matter density during the postbounce evolution phase. On the other hand, an off-center population of thermal Λ hyperons is the result of peak values of temperature away from the center of the PNS. When we set the neutrino heating scale factor $f_{\rm heat} = 1$, each CCSN simulation ends with the formation of a black hole driven by mass accretion. It is interesting to find out that the black hole formation time for the BHB$\Lambda\phi$ EOS is shorter than that of the HShen Λ EOS, though the opposite conclusion is drawn from the accretion-driven black hole with the HShen nuclear and HS (DD2) EOS models. This is attributed to the fact that the repulsive Λ–Λ interaction in the BHB$\Lambda\phi$ EOS makes it a stiffer EOS than the HShen Λ EOS. Neutrino luminosity is found to cease with the formation of a black hole earlier for the Λ hyperon EOS than for the corresponding case with the nuclear EOS. We have studied the metastability of the PNS due to the BHB$\Lambda\phi$ EOS in the long-duration evolution after a successful supernova explosion using the s20WH07 progenitor model with the increased neutrino heating scale factor of $f_{\rm heat} = 1.5$. In this case we do not find any delayed collapse into the black hole due to the presence of Λ hyperons in the PNS. The PNS that has a mass $\sim$1.64 $M_\odot$ remains stable until 4 s and might become a cold neutron star.

The numerical calculations presented in this article have been performed in the blade server of the Astroparticle Physics and Cosmological Division, Saha Institute of Nuclear Physics. We acknowledge fruitful discussions of GR1D with Evan O'Connor. D.B. thanks the Alexander von Humboldt Foundation for support.

REFERENCES

Antoniadis, J., Freire, P. C. C., Wex, N., et al. 2013, Sci, 340, 448
Banik, S., & Bandyopadhyay, D. 2001, PhRvC, 63, 035802
Banik, S., & Bandyopadhyay, D. 2002, PhRvC, 66, 065801
Banik, S. 2013, JPhCS, 426, 12004
Banik, S. 2014, PhRvC, 89, 035807
Banik, S., Hempel, M., & Bandyopadhyay, D. 2014, ApJS, 214, 22
Baumgarte, T. W., Janka, H. Th., Keil, W., Shapiro, S. L., & Teukolsky, S. A. 1996, ApJ, 468, 823
Brown, G. E., & Bethe, H. A. 1994, ApJ, 423, 659
Buballa, M., Dexheimer, V., Drago, A., et al. 2014, J. Phys. G, 41, 123001
Char, P., & Banik, S. 2014, PhRvC, 90, 015801
Colucci, G., & Sedrakian, A. 2013, PhRvC, 87, 055806
Dover, C. B., & Gal, A. 1985, PrPNP, 12, 171
Fischer, T., Hempel, M., Sagert, I., Suwa, Y., & Schaffner-Bielich, J. 2014, EPJA, 50, 46
Fischer, T., Whitehouse, S. C., Mezzacappa, A., Thielemann, F.-K., & Liebendörfer, M. 2009, A&A, 499, 1
Gusakov, M. E., Haensel, P., & Kantor, E. M. 2014, MNRAS, 439, 318
Hempel, M., & Schaffner-Bielich, J. 2010, NuPhA, 837, 210
Ishizuka, C., Ohnishi, A., Tsubakihara, K., Sumiyoshi, K., & Yamada, S. 2008, J. Phys. G, 35, 085201
Janka, H.-T. 2001, A&A, 368, 527
Keil, W., & Janka, H. Th. 1995, ApJ, 296, 145
Lattimer, J. M., & Lim, Y. 2013, ApJ, 771, 51
Lattimer, J. M., & Swesty, F. D. 1991, NuPhA, 535, 331
Lastowiecki, R., Blaschke, H., Grigorian, H., & Typel, S. 2012, AcPP, 5, 535
Lonardoni, D., Lovato, A., Gandolfi, S., & Pederiva, F. 2015, PhRvL, 114, 092301
Lopes, L. L., & Menezes, D. P. 2013, PhRvC, 89, 025805
Mares, J., Friedman, E., Gal, A., & Jennings, B. 1995, NuPhA, 594, 311
Millener, D. J., Dover, C. B., & Gal, A. 1988, PhRvC, 38, 2700
Nakazato, K., Furusawa, S., Sumiyoshi, K., et al. 2012, ApJ, 745, 197
Nakazato, K., Sumiyoshi, K., & Yamada, S. 2008, PhRvD, 77, 103006
O'Connor, E., & Ott, C. 2010, CQGra, 27, 114103
O'Connor, E., & Ott, C. 2011, ApJ, 730, 70
Oertel, M., Fantina, A. F., & Novak, J. 2012, PhRvC, 85, 055806
Peres, B., Oertel, M., & Novak, J. 2013, PhRvD, 87, 043006
Prakash, M., Cooke, J. R., & Lattimer, J. M. 1995, PhRvD, 52, 661
Rosswog, S., & Liebendörfer, M. 2003, MNRAS, 342, 673
Ruffert, M., Janka, H.-T., & Schaf˙er, G. 1996, A&A, 311, 532
Sagert, I., Fischer, T., Hempel, M., Pagliara, G., & Schaffner-Bielich, J. 2009, PhRvL, 102, 081101
Schaffner, J., & Mishustin, I. N. 1996, PhRvC, 53, 1416
Schaffner, J., Stöcker, H., & Greiner, C. 1992, PhRvC, 46, 322
Shen, H., Toki, H., Oyamatsu, K., & Sumiyoshi, K. 1998, NuPhA, 637, 435
Shen, H., Toki, H., Oyamatsu, K., & Sumiyoshi, K. 2011, ApJS, 197, 20
Sugahara, Y., & Toki, H. 1994, NuPhA, 579, 557
Sumiyoshi, K., Ishizuka, C., Ohnishi, A., Yamada, S., & Suzuki, H. 2009, ApJL, 690, L43
Sumiyoshi, K., Yamada, S., & Suzuki, H. 2007, ApJ, 667, 382
Typel, S., Röpke, G., Klähn, T., Blaschke, D., & Wolter, H. H. 2010, PhRvC, 81, 015803
Typel, S., & Wolter, H. H. 1999, NuPhA, 656, 331
Typel, S., Oertel, M., & Klaehn, T. 2013, arXiv:1307.5715
van Dalen, E. N. E., Colucci, G., & Sedrakian, A. 2014, PhLB, 734, 383
Weissenborn, S., Chatterjee, D., & Schaffner-Bielich, J. 2012a, NuPhA, 881, 62
Weissenborn, S., Chatterjee, D., & Schaffner-Bielich, J. 2012b, PhRvC, 85, 065802
Woosley, S. E., & Heger, A. 2007, PhR, 442, 269
Woosley, S. E., Heger, A., & Weaver, T. A. 2002, RvMP, 75, 1015
Woosley, S. E., & Weaver, T. A. 1995, ApJS, 101, 181